

Excitation energy division in heavy-ion reactions

H. Madani, A. C. Mignerey, A. A. Marchetti,^{*} A. P. Weston-Dawkes,[†] and W. L. Kehoe[‡]
University of Maryland, College Park, Maryland 20742

F. Obenshain

Oak Ridge National Laboratory, Oak Ridge, Tennessee 37831

(Received 11 January 1996)

The excitation energy of the primary products from the reaction ^{56}Fe on ^{165}Ho at 672 MeV was determined by the kinematic coincidence technique. The fraction of the total excitation energy of the system stored in the projectilelike fragment was found to decrease with increasing energy loss. However, thermal equilibrium is not reached, even at the highest energy damping. A small correlation between excitation energy partition and reaction exit channel was observed. Monte Carlo simulations of the present experiment confirmed that some of this correlation is due to the finite resolution of the measured parameters. [S0556-2813(96)05808-6]

PACS number(s): 25.70.Lm, 24.10.Lx

I. INTRODUCTION

One salient feature of deep-inelastic heavy-ion reactions is the conversion of relative kinetic energy of the system into excitation energy. Knowledge of how this excitation energy is divided between the two reaction partners is important to the understanding of the underlying mechanisms. However, since the primary fragments are short lived (10^{-18} – 10^{-16} s), the excitation energy of the composite system formed after the collision cannot be measured directly; it has to be inferred from other observables.

Various techniques have been used to determine the excitation energy of the reaction fragments [1–11]. A kinematic coincidence technique in which the projectilelike fragment (PLF) and the targetlike fragment (TLF) are detected simultaneously was one of the first methods tried in the 1970s for excitation energy determination [1]. Based on the assumption that deep-inelastic reactions are binary, and that the average fragment scattering angle and velocity are unchanged by evaporation, the PLF primary mass (preevaporation) can be evaluated from measured secondary (postevaporation) quantities. The use of an evaporation code then allows the determination of the excitation energy of the PLF. The results obtained by Babinet *et al.* [1] suggested that thermal equilibrium, where the temperatures τ_{PLF} and τ_{TLF} of the PLF and the TLF are equal, was attained by the two fragments and, therefore, the excitation energy of the system was divided according to the mass ratios of the reaction fragments.

Other experiments based on the detection of neutrons emitted from the PLF and the TLF were performed. One example is the study of the 400-MeV Cu+Au system by Tamain *et al.* [6], which confirmed the finding of thermal equilibrium in deep-inelastic reactions. However, studies of the system $^{58}\text{Ni} + ^{197}\text{Au}$ at 15.3 MeV/u by Awes *et al.* [12]

showed an important disagreement with the previous conclusions. In this case only the projectilelike fragments were detected and the excitation energy division was inferred from comparing PLF charge distributions to theoretical distributions obtained by applying evaporation corrections to primary distributions predicted by Randrup's nucleon exchange model [13]. The results in this case seemed to be more consistent with the scenario where the excitation energy is divided equally between the two fragments at small energy losses (less than 100 MeV) and tends to a mass partition for higher values of energy loss. However, the predictions were based on primary distributions which do not have the strong negative charge drift exhibited by the experimental data. Therefore, it is not possible to make any rigorous conclusions.

The study of the 505-MeV ^{56}Fe on ^{165}Ho system with the kinematic coincidence technique by Benton *et al.* [8] showed an evolution of the system from equal excitation energy division at low total kinetic energy loss (TKEL) towards a division according to the fragment masses at higher TKEL. However, no evidence of reaching thermal equilibrium was observed.

Another question addressed in the various studies of excitation energy division is the correlation between fragment mass and energy partition. This feature was reported by Sohlbach *et al.* [9] in the study of the reaction ^{208}Pb on ^{86}Kr at 10, 13, and 18.2 MeV/u and which showed that the heavier fragment was more excited than the lighter one. In addition, the correlation was found to decrease with increasing excitation energy.

The fragment mass-energy partition correlation was also observed for the reaction ^{56}Fe on ^{165}Ho at 505 MeV by Benton *et al.* [8] and the reaction ^{74}Ge on ^{165}Ho at 629 MeV by Kwiatkowski *et al.* [10]. These two studies showed that in both systems the PLF is hotter than the TLF for pickup reactions ($A'_{\text{PLF}} > A$ of the projectile) at low energy damping. The opposite is true for stripping reactions ($A'_{\text{PLF}} < A$ of the projectile). The mass dependence was found to be weaker at higher dissipation energies. However, it was suggested by Töke *et al.* [14] that the correlation can be attributed to instrumental effects. Monte Carlo simulations were performed

^{*}Present address: Lawrence Livermore National Laboratory, Livermore, CA 94550.

[†]Present address: Department of Energy, Washington, DC 20585.

[‡]Present address: 86 Buckingham, Cambridge, MA 02138.

to reproduce the parameters and the resolution of the experimental setup. The results of the simulation for the ^{74}Ge on ^{165}Ho system showed that some of the excitation energy division dependence on the primary mass of the projectile was indeed due to finite resolutions of some of the measured variables [15]. However, these instrumental effects could not account for all of the correlation between excitation energy sharing and exit channel.

The primary goal of the present study of the 672-MeV ^{56}Fe on ^{165}Ho system is to address the question of how the excitation energy of the system is partitioned between the two complex fragments that are emitted in deep-inelastic collisions. The use of the coincidence method to detect both reaction fragments, the PLF and the TLF, provides less ambiguous characterization of the PLF in terms of its preevaporative mass than when relying on excitation energy division assumptions to obtain postevaporative results from model predictions of primary fragments. This, in turn, makes the determination of the PLF excitation energy by this type of analysis more rigorous than by analyses based on the study of mass and charge distributions of secondary fragments.

The kinematic coincidence technique is based on the assumption that the detected fragments are close in mass and charge to the primary fragments before deexcitation, and on the premise that the only way the reaction products dispose of their excitation energy is via evaporation and gamma ray emission, processes which can be simulated by well tested statistical models. Therefore, it is important to choose reaction partners that are not likely to undergo fission. The ^{56}Fe on ^{165}Ho system is thus an adequate choice, as both Fe and Ho are not heavy enough to have a significant fission cross section at the expected excitation energies. In addition, since this system is asymmetric, it is easy to determine whether the system attains thermal equilibrium by studying the ratio of the PLF excitation energy to the total excitation energy of the system.

The ^{56}Fe on ^{165}Ho system has been extensively studied by other authors at various bombarding energies and with different experimental methods. Therefore, it is useful to compare the results of the present study to previous results and add to the already existing pool of knowledge about this system. It is particularly worthwhile to compare the present results to those obtained by Benton *et al.* [8] for the same reaction at lower bombarding energy and using the same kinematic coincidence method. The study of the 672-MeV ^{56}Fe on ^{165}Ho system constitutes, in fact, a continuation of the study of the same system at 505 MeV bombarding energy, and allows for exploration of a wider range of total kinetic energy loss.

II. EXPERIMENTAL TECHNIQUE AND DATA REDUCTION

A. Experimental setup

The experiment was performed at the Holifield Heavy Ion Research Facility (HHIRF) with a ^{56}Fe beam of $E/A=12$ MeV impinging on a carbon-backed ^{165}Ho target. The PLF energy, charge, mass, and scattering angle were measured using a time-of-flight arm consisting of 2 parallel plate avalanche counters (PPAC's) and a 4-anode ionization chamber.

A detailed description of the experimental and calibration techniques for characterizing the PLF can be found in Refs. [16] and [17].

The TLF's were detected using a PPAC positioned inside the scattering chamber, and referred to as the recoil PPAC, providing the TLF horizontal (x -) and vertical (y -) positions, which were translated into in-plane and out-of-plane TLF scattering angles, respectively. The recoil PPAC was mounted 375 mm from the target and subtended an in-plane angle of 75° . With this positioning, it covered angles ranging from a minimum of 15° to a maximum of 90° . The recoil PPAC was filled with isobutane at a pressure of 4.0 torr.

A mask consisting of a square aluminum plate of 10 cm by 10 cm with equally spaced holes was placed in front of the recoil detector during a calibration run, and was used for the calibration of the TLF scattering angle. To determine the angular position of the holes, the calibration mask was placed in front of the beam line, at 0° with respect to the beam. Each of the ten in-plane holes was then viewed through a transit line and its relative angular position recorded. The absolute angular differences between consecutive holes could then be determined and used in the angular calibration. A gold target was used during the TLF angle calibration run to maximize the elastic cross section.

B. Primary PLF mass and excitation energy determination

The kinematic coincidence technique, where the PLF and the TLF are detected in coincidence, was used to extract information about the primary reaction fragments before evaporation takes place. One basic assumption in this technique is the invariance, on the average, of the velocity and scattering angle of the emitted fragment by particle evaporation. Assuming the validity of this assumption, which is based on the statistical properties of evaporation, the PLF primary mass can be obtained by the application of two-body kinematics. For nonrelativistic cases, momentum conservation is expressed by the two equations

$$P_{\text{proj}} = P_{\text{PLF}} \cos(\theta_{\text{PLF}}) + P_{\text{TLF}} \cos(\theta_{\text{TLF}}), \quad (1)$$

and

$$P_{\text{PLF}} \sin(\theta_{\text{PLF}}) = P_{\text{TLF}} \sin(\theta_{\text{TLF}}), \quad (2)$$

where P_{proj} is the projectile momentum, P_{PLF} and P_{TLF} are the momenta of the PLF and the TLF, respectively, and θ_{PLF} and θ_{TLF} are their respective scattering angles. Classically, the linear momentum \vec{P} of a particle of mass M traveling with a velocity \vec{V} is

$$\vec{P} = M \vec{V}. \quad (3)$$

Using the scalar values of momentum and velocity the mass of the PLF can thus be written as

$$M_{\text{PLF}} = M_{\text{proj}} \frac{V_{\text{proj}}}{V_{\text{PLF}} [\cos(\theta_{\text{PLF}}) + \sin(\theta_{\text{PLF}}) \cot(\theta_{\text{TLF}})]}, \quad (4)$$

where M_{proj} and V_{proj} are the projectile mass and velocity, and V_{PLF} is the PLF velocity. All the parameters in Eq. (4)

are either known exactly, or assumed to be unchanged, on the average, by particle evaporation; therefore, the primary mass of the PLF can be determined with a fairly good approximation. The mass evaporated from the PLF, ΔA , can then be determined by subtracting the measured mass from the primary mass as calculated from Eq. (4). The evaporated mass ΔA was used with results of the evaporation code PACE II to compute the PLF excitation energy. An iterative procedure developed by Benton *et al.* [8] and later used by Kwiatkowski *et al.* [10], was utilized and is briefly described here. More details about this technique can be found in Refs. [8] and [10].

The amount of evaporated charge ΔZ and evaporated mass ΔA from a primary PLF with atomic number Z'_{PLF} , mass number A'_{PLF} , and excitation energy E^*_{PLF} can be expressed as a function of Z'_{PLF} , A'_{PLF} , and E^*_{PLF} and the secondary PLF mass A''_{PLF} and charge Z''_{PLF} by the two equations

$$\Delta A_{\text{PLF}} = A'_{\text{PLF}} - A''_{\text{PLF}} = f_{\Delta A}(Z'_{\text{PLF}}, A'_{\text{PLF}}, E^*_{\text{PLF}}), \quad (5)$$

and

$$\Delta Z_{\text{PLF}} = Z'_{\text{PLF}} - Z''_{\text{PLF}} = f_{\Delta Z}(Z'_{\text{PLF}}, A'_{\text{PLF}}, E^*_{\text{PLF}}). \quad (6)$$

The quantities ΔA_{PLF} and ΔZ_{PLF} are generated by running the evaporation code PACE II. The results are tabulated and stored as computer files, which will be referred to as the ΔA and ΔZ tables. To generate these tables, the evaporation code was run for 26 isotopes of each element with atomic numbers between 10 and 35 and for excitation energies between 0 and 300 MeV. Steps of 10 MeV were used for excitation energies lower than 100 MeV, and 50-MeV steps were used for higher excitation energies. The functions $f_{\Delta A}(Z'_{\text{PLF}}, A'_{\text{PLF}}, E^*_{\text{PLF}})$ and $f_{\Delta Z}(Z'_{\text{PLF}}, A'_{\text{PLF}}, E^*_{\text{PLF}})$ were then determined by interpolation of the values calculated for the chosen set of Z , A , and E^* values that were obtained using PACE II. Therefore, the excitation energy and the primary charge of the PLF can be evaluated using results from the evaporation code PACE II. In Eqs. (5) and (6), the three unknowns are Z'_{PLF} , ΔZ_{PLF} , and E^*_{PLF} . They were determined by employing a self-consistent iteration procedure in which Eqs. (5) and (6) were solved event-by-event at each iteration. Starting at an assumed value for Z'_{PLF} , the value of $E^*_{\text{PLF}}(i)$ at each iteration (i) was determined by solving Eq. (5). It is then possible to solve Eq. (6) for ΔZ_{PLF} . The convergence of the iteration was reached when

$$e(i) = |\Delta Z_{\text{PLF}}(i) - \Delta Z_{\text{PLF}}(i-1)| < 0.1. \quad (7)$$

For events that did not satisfy inequality (7), the convergence was accelerated by defining a new value for $Z'_{\text{PLF}}(i)$ as

$$Z'_{\text{PLF}}(i) = Z'_{\text{PLF}}(i-1) + 0.9e(i). \quad (8)$$

Only events with positive values of ΔA_{PLF} were selected, and the maximum number of iterations allowed was 20.

A contour plot of the excitation energy of the PLF versus TKEL is displayed in Fig. 1(a). The limits of no TLF excitation energy, equal sharing of the excitation energy by the PLF and the TLF, and thermal equilibrium, are indicated by the dotted, dashed, and solid lines, respectively. Most of the events are in the region comprised by the $E^*_{\text{TLF}} = 0$ limit and

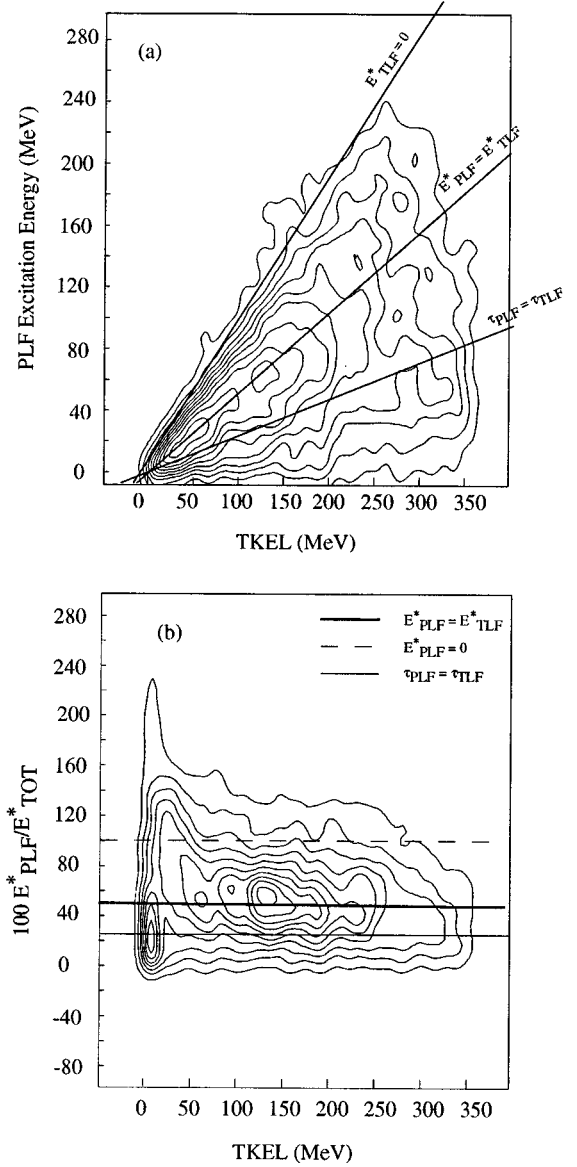


FIG. 1. Contour plot of (top) the PLF excitation energy and (bottom) the PLF excitation energy ratio as a function of TKEL for the 672-MeV ^{56}Fe on ^{165}Ho reaction. The limits of nonexcited TLF, equipartition of the excitation energy, and thermal equilibrium are indicated by the straight lines.

the thermal equilibrium limit. Another parameter of interest, which describes the excitation energy division more directly, is the ratio of the PLF excitation energy to the total excitation energy, $E^*_{\text{PLF}}/E^*_{\text{tot}}$. The quantity $E^*_{\text{PLF}}/E^*_{\text{tot}}$ is defined as a percentage and is therefore expected to have values between 0% and 100%. Any values outside this range are not physically possible. The PLF excitation energy ratio $E^*_{\text{PLF}}/E^*_{\text{tot}}$ is plotted against TKEL in Fig. 1(b). The values of the $E^*_{\text{PLF}}/E^*_{\text{tot}}$ ratio are between 0% and 100% for most of the events. Slit scattering and events with negative evaporated mass have been eliminated. The limits where all the excitation energy is in the PLF, the equal sharing of the excitation energy and the thermal equilibrium limits are again indicated by the dotted, dashed, and solid lines, respectively. The high yield shown at TKEL values around 0 MeV is due to contributions from elastic scattering. The distribu-

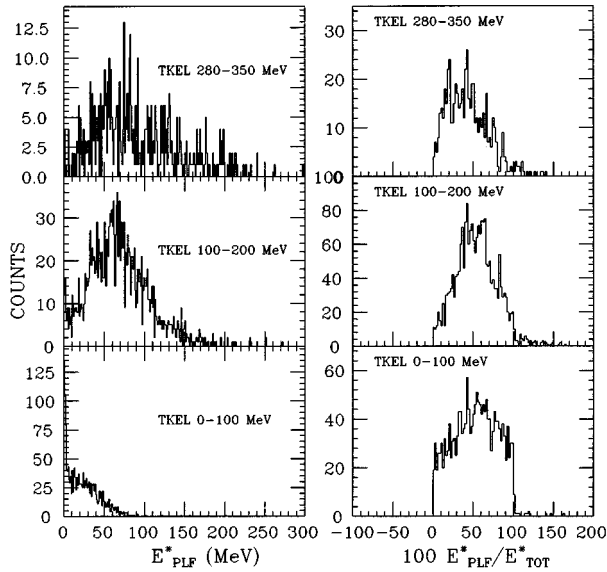


FIG. 2. Histograms of the PLF excitation energy (left) and excitation energy ratio (right) for three representative gates of TKEL, for the 672-MeV ^{56}Fe on ^{165}Ho reaction.

tions of E_{PLF}^* and E_{PLF}^*/E_{TOT}^* for different bins of TKEL have approximately Gaussian shapes, as shown in Fig. 2. Therefore, Gaussian fits were performed to extract the centroids and widths of these distributions. It is also possible to use a one-dimensional moment analysis approach. However, in this case it is essential to ensure the exclusion of any long tails from the calculation. Both methods were tested and gave similar results for well defined peaks, while it was better to use Gaussian fits for cases of low counts. Therefore,

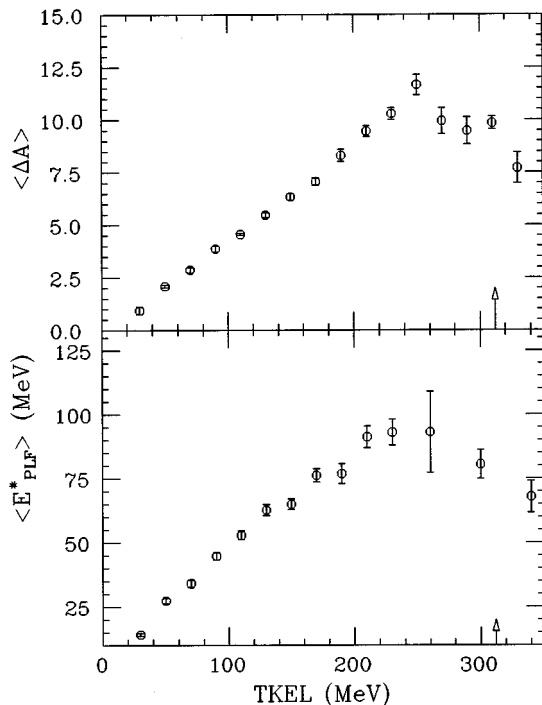


FIG. 3. Centroids of ΔA the mass evaporated from the PLF, and the PLF excitation energy, E_{PLF}^* as a function of TKEL, for the 672-MeV ^{56}Fe on ^{165}Ho reaction.

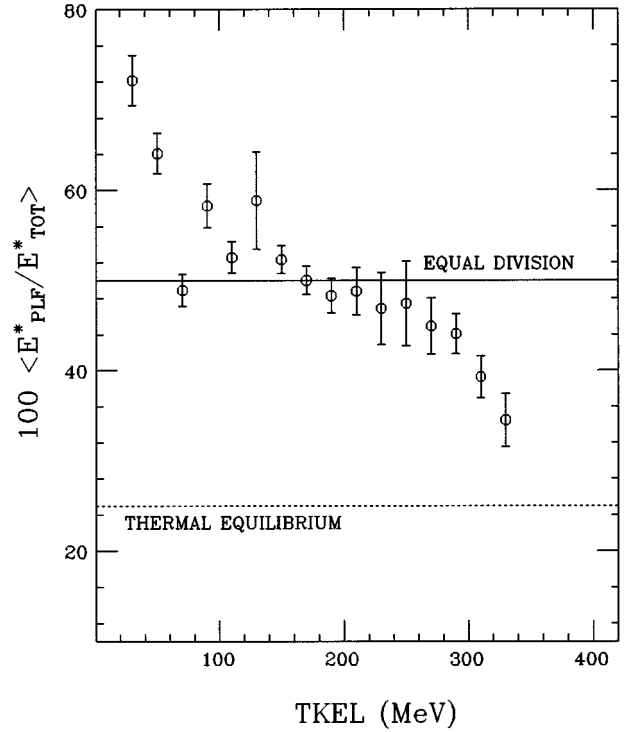


FIG. 4. The PLF excitation energy ratio F_{PLF}^*/E_{TOT}^* as a function of energy loss for inclusive isotopes, for the reaction ^{56}Fe on ^{165}Ho at 672 MeV. Equal excitation energy division and thermal equilibrium are indicated by the solid and dashed lines, respectively.

the Gaussian-fit method was opted for in the present study. Because of the low statistics, it was not possible to obtain reliable values for the widths of the E_{PLF}^* and E_{PLF}^*/E_{TOT}^* distributions, therefore, these are not presented.

III. EXCITATION ENERGY DIVISION

The evolution of the PLF excitation energy with the total kinetic energy loss, TKEL, is shown in Fig. 3(a) for the ^{56}Fe on ^{165}Ho reaction. The values of $\langle E_{PLF}^* \rangle$ increase almost linearly with increasing energy loss. A maximum value of about 93 MeV is reached at 260 MeV of TKEL. However, this apparent lowering of $\langle E_{PLF}^* \rangle$ for $\text{TKEL} > 260$ MeV could be attributed to a less accurate determination of the centroids at high values of TKEL, where only few events occur, as suggested by the increased errors.

The average mass evaporated from the PLF $\langle \Delta A \rangle$ was also determined with one-dimensional Gaussian fits, as a function of TKEL. The ΔA centroids are displayed in Fig. 3 as a function of TKEL. The behavior of $\langle \Delta A \rangle$ with TKEL is similar to that of E_{PLF}^* . A maximum of 12 mass units is reached at 250 MeV of TKEL. A slight decrease is shown at TKEL higher than 250 MeV, but again the statistical errors are large in this region.

The evolution of the $\langle E_{PLF}^* / E_{TOT}^* \rangle$ with TKEL is shown in Fig. 4. The ratios corresponding to the limits of equal excitation energy division and thermal equilibrium are indicated by the solid and dashed lines, respectively. The value of $\langle E_{PLF}^* / E_{TOT}^* \rangle$ exceeds the limit of equal excitation energy di-

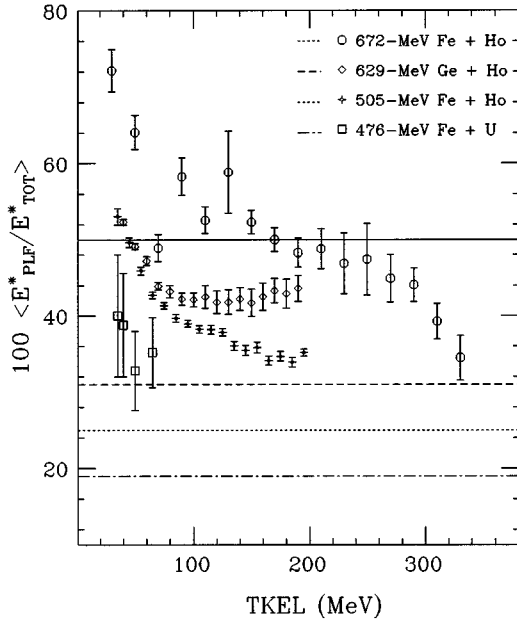


FIG. 5. The PLF excitation energy ratio as a function of energy loss for inclusive isotopes, for the reactions ^{56}Fe on ^{165}Ho at 505 MeV and 672 MeV, ^{56}Fe on ^{238}U at 476 MeV, and ^{74}Ge on ^{165}Ho at 629 MeV. The solid line refers to equal excitation energy division. The short-dashed, long dashed, and dot-dashed lines refer to thermal equilibrium for ^{56}Fe on ^{165}Ho at 505 MeV, and 672 MeV, ^{74}Ge on ^{165}Ho at 629 MeV, and ^{56}Fe on ^{238}U , respectively.

vision for TKEL values below 120 MeV and remains nearly constant around 50% for TKEL values between 120 MeV and 260 MeV. A sharp decrease in $\langle E_{\text{PLF}}^*/E_{\text{tot}}^* \rangle$ is observed above 260 MeV of TKEL. However, the thermal equilibrium limit is never reached.

The kinematic coincidence technique was used in the study of the 505-MeV ^{56}Fe on ^{165}Ho system by Benton *et al.* [8] and the 629-MeV ^{74}Ge on ^{165}Ho system by Planeta *et al.* [4]. The results for the Fe+Ho system suggest that equal sharing of the excitation energy is favored at low energy losses (< 50 MeV), whereas for larger energy losses the data show a tendency towards a division according to mass ratios. However, there was no evidence of thermal equilibrium, even at the highest energy loss values [8]. A qualitatively similar behavior was shown by the data of the Ge+Ho system [10]. The $\langle E_{\text{PLF}}^*/E_{\text{tot}}^* \rangle$ ratios obtained with these two systems are compared to those obtained in the present study of the 672-MeV $^{56}\text{Fe} + ^{165}\text{Ho}$ system in Fig. 5. Results obtained with the 476-MeV $^{56}\text{Fe} + ^{238}\text{U}$ by Vandenbosch *et al.* [7] are also shown. The limits of equal division and thermal equilibrium for each system are as indicated. One remarkable feature is the higher $\langle E_{\text{PLF}}^*/E_{\text{tot}}^* \rangle$ values for the systems with higher bombarding energy. A possible explanation could be the higher relative velocity, or a shorter interaction time.

IV. MASS DEPENDENCE OF EXCITATION ENERGY DIVISION

The correlation between excitation energy division and exit channel is shown in Fig. 6, where the $E_{\text{PLF}}^*/E_{\text{tot}}^*$ cen-

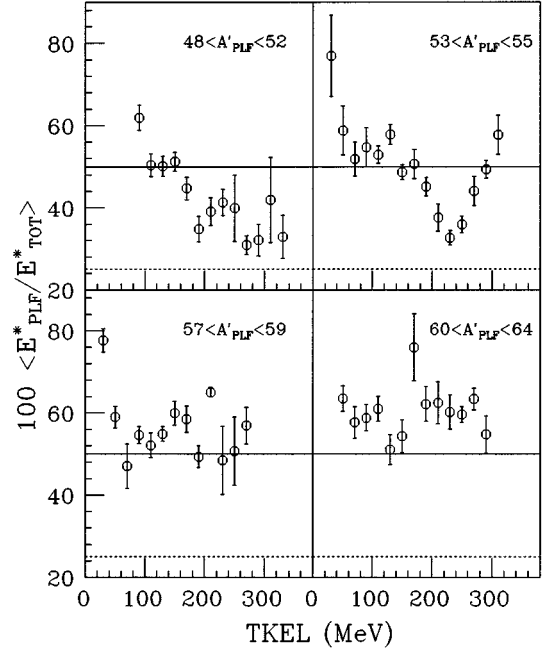


FIG. 6. Centroids of the PLF excitation energy ratio $E_{\text{PLF}}^*/E_{\text{tot}}^*$ as a function of TKEL for different gates of primary PLF mass (A'_{PLF}), for the 672-MeV ^{56}Fe on ^{165}Ho reaction. The limits of equipartition of the excitation energy and thermal equilibrium are indicated by the solid and dotted lines, respectively.

troids are plotted versus TKEL for selective bins of primary (pre-evaporation) PLF mass, A'_{PLF} . Figure 6 shows that the contribution to the low $E_{\text{PLF}}^*/E_{\text{tot}}^*$ ratios at low TKEL is mostly due to events with primary masses lower than 56, the mass of the projectile. For primary masses higher than 56, the values of the PLF excitation energy ratio are in the 50% to 70% range at all values of TKEL. An alternative way of looking at the correlation between the excitation energy ratio $E_{\text{PLF}}^*/E_{\text{tot}}^*$ and the exit channel is by plotting $E_{\text{PLF}}^*/E_{\text{tot}}^*$ versus A'_{PLF} and versus A''_{PLF} .

To obtain the $E_{\text{PLF}}^*/E_{\text{tot}}^*$ ratio as a function of A'_{PLF} and A''_{PLF} , the spectra of $E_{\text{PLF}}^*/E_{\text{tot}}^*$ ratio were generated for consecutive bins of A'_{PLF} and A''_{PLF} , and their centroids determined by Gaussian fits. Since the mass of the secondary PLF, A''_{PLF} , is evaluated more accurately than the primary PLF mass A'_{PLF} , the $E_{\text{PLF}}^*/E_{\text{tot}}^*$ ratio is also determined as a function of A''_{PLF} . The results are displayed in Fig. 7.

The dotted lines in Fig. 7 describe how the excitation energy would be divided if the fragments were in thermal equilibrium. In this case the excitation energy is determined as a function of the fragment mass (A'_{PLF} or A''_{PLF}). The excitation energy of a projectile-like fragment (or any excited nucleus) can be written in terms of its mass and nuclear temperature τ as

$$E_{\text{PLF}}^* = a_{\text{PLF}} \tau_{\text{PLF}}^2, \quad (9)$$

where a_{PLF} is the level density parameter, assumed to be proportional to the PLF mass. Equation (9) is also valid for the targetlike fragment. Therefore, when the two fragments have equal temperatures, the total excitation energy of the system is expressed as

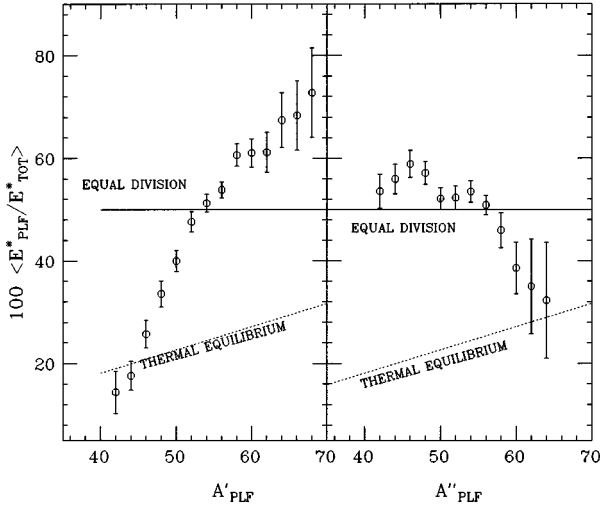


FIG. 7. Centroids of the PLF excitation energy ratio E_{PLF}^*/E_{tot}^* as a function of the primary PLF mass (A'_{PLF}) and secondary PLF mass (A''_{PLF}) for inclusive events, for the 672-MeV ^{56}Fe on ^{165}Ho reaction elastic and slit-scattering events are gated out. The limits of equipartition of the excitation energy and thermal equilibrium are indicated by the solid and dotted lines, respectively.

$$E_{tot}^* = E_{PLF}^* + E_{TLF}^* = (a_{PLF} + a_{TLF})\tau^2. \quad (10)$$

The ratio of the PLF excitation energy to the total excitation energy as a function of the PLF mass can thus be derived from Eq. (10), and expressed as

$$E_{PLF}^*/E_{tot}^* = A'_{PLF}/A_{tot}. \quad (11)$$

For the ^{56}Fe on ^{165}Ho system, $A_{tot} = 221$ and therefore,

$$E_{PLF}^*/E_{tot}^* \times 100 = 0.452A'_{PLF}. \quad (12)$$

The thermal equilibrium limit determined in this fashion is more accurate than the constant value of 25% used in Figs. 4 and 5. In those cases it was necessary to assume a constant value for A'_{PLF} . Since the primary PLF mass was found not to decrease greatly with TKEL, the mass of the projectile was used. An evolution of the system from thermal equilibrium at low values of A'_{PLF} towards E_{PLF}^*/E_{tot}^* values even higher than the equipartition of the excitation energy limit with increasing A'_{PLF} is observed in Fig. 7. In contrast, when plotted against the secondary PLF mass (A''_{PLF}), the E_{PLF}^*/E_{tot}^* ratio indicates that the excitation energy is shared nearly equally by the two fragments for A''_{PLF} values lower than 56. Above A''_{PLF} of 56, the E_{PLF}^*/E_{tot}^* ratio decreases towards values approaching thermal equilibrium. However, it is important to remember that the secondary mass gives a picture of the system after deexcitation. The PLF excitation energy ratios versus A'_{PLF} and A''_{PLF} for different bins of energy loss are displayed in Fig. 8. A slight dependence of the E_{PLF}^*/E_{tot}^* ratio on A'_{PLF} is observed in Fig. 8 (left panel) for the three selected bins of TKEL. A different scenario is observed when the PLF excitation energy ratio is plotted as a function of A''_{PLF} as shown in Fig. 8(a). For the low and the intermediate TKEL bins, the E_{PLF}^*/E_{tot}^* ratio shows a slight parabolic dependence on A''_{PLF} . At the highest TKEL bin, the

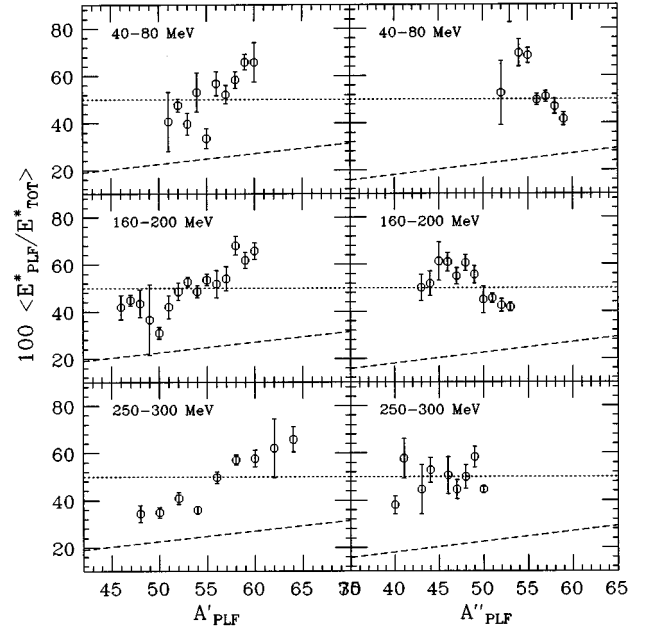


FIG. 8. Centroids of the PLF excitation energy ratio (E_{PLF}^*/E_{tot}^*) as a function of the primary PLF mass (A'_{PLF}) and the secondary PLF mass (A''_{PLF}) for three TKEL gates, for the 672-MeV ^{56}Fe on ^{165}Ho reaction. The limits of equipartition of the excitation energy and thermal equilibrium are indicated by the dotted and dashed lines, respectively.

excitation energy seems to be divided nearly equally between the two reaction fragments at all values of A''_{PLF} .

The study of the 629-MeV $^{74}\text{Ge} + ^{165}\text{Ho}$ system by Kwiatkowski *et al.* [10] showed that the dependence of excitation energy sharing on the primary fragment mass weakens with increasing energy loss. This feature is not noticeable in the 672-MeV $^{56}\text{Fe} + ^{165}\text{Ho}$ system.

V. MONTE CARLO SIMULATIONS

The dependence of excitation energy division on the direction of transfer has been observed in the present study and has also been reported for reactions. However, such a strong correlation cannot be fully attributed to physical phenomena and systematic errors and instrumental effects may contribute to the mass dependence, as was suggested by Töke *et al.* [14]. To investigate the sensitivity of the E_{PLF}^*/E_{tot}^* centroids to these effects, Monte Carlo simulations of the experiment for the 505-MeV $^{56}\text{Fe} + ^{165}\text{Ho}$ reaction [8] were performed by Töke *et al.* [14]. A very good agreement between the experimental data and the Monte Carlo results was observed starting with a mass-independent division of the excitation energy, it could thus be implied that the kinematic coincidence technique is responsible for the correlations between fragment mass and excitation energy. This was thought to be due to the finite mass resolutions of the detected fragments [14].

Similar Monte Carlo simulations based on Refs. [10] and [14] were used to model the 672-MeV $^{56}\text{Fe} + ^{165}\text{Ho}$ experiment. The parameters that define the reaction, such as mass and charge of the projectile and target, the laboratory bombarding energy, and the detector angular acceptances, were

used as inputs to the Monte Carlo code. Other inputs related to the instrumentation are the experimental resolutions in PLF mass and charge, estimated to be 1.3 and 0.3, respectively, and the resolution in the TLF angle (2.5°) and PLF angle (0.5°). These are introduced in the code to reproduce as closely as possible the experimental conditions.

The first step in the Monte Carlo simulation procedure was the generation of primary nuclide distributions (in the N - Z plane in this case) that would describe the primary distribution of PLF's emitted in the reaction in question. The characteristic centroids and widths of the primary PLF mass and charge distributions obtained experimentally by the kinematic reconstruction technique were employed to generate the "simulated" primary N - Z distributions. This ensures that the measured events are reproduced by the "simulated" secondary events before the kinematic reconstruction. A further comparison of real and simulated data would otherwise be meaningless. The direction of the preevaporated fragments emitted in the reaction was described by a center-of-mass angular distribution

$$\frac{d\sigma}{d\Omega} \propto \frac{1}{\sin\theta_{c.m.}}. \quad (13)$$

The secondary nuclide distributions, equivalent to those measured experimentally, were obtained by subjecting the primary distributions to evaporation corrections using results from PACE II. At this point, it was necessary to make assumptions about the excitation energy of the PLF, since it is required as an input to PACE II. Two different hypotheses were investigated: a sharing of the excitation energy independent of the primary PLF mass, where the average value of the $E_{\text{PLF}}^*/E_{\text{tot}}^*$ ratio obtained experimentally ($\approx 50\%$) was used, and a mass-dependent division based on the experimental results.

The recoil effects due to particle evaporation from the emitted fragments were taken into account and the distribution of the recoil velocities was simulated by a Maxwellian formulation [18]. The mass and charge resolution of the secondary PLF, as well as the velocity vectors of the secondary PLF and TLF, were randomized to reproduce the finite mass, charge and angular resolutions that were measured experimentally. The secondary distributions obtained in this fashion were characterized by the same parameters as the experimental distributions: PLF mass, charge, kinetic energy and angle, and TLF angle. The simulated data were then analyzed in a way identical to the analysis of the experimental events, and the PLF excitation energy ratios that were determined from these calculations were compared to the experimental results.

Before comparing the experimental $E_{\text{PLF}}^*/E_{\text{tot}}^*$ ratios to the values obtained from the simulation, it was necessary to verify that the experimental nuclide distributions were reproduced by the Monte Carlo procedure. The centroids and variances of the secondary N and Z distributions obtained with the simulated data are compared to those of experimental distributions in Fig. 9. The centroids are well reproduced by the simulation. However, the variances for the simulated events are higher than the experimental ones. A similar comparison is made between the centroids and variances of the simulated reconstructed primary distribution and the experi-

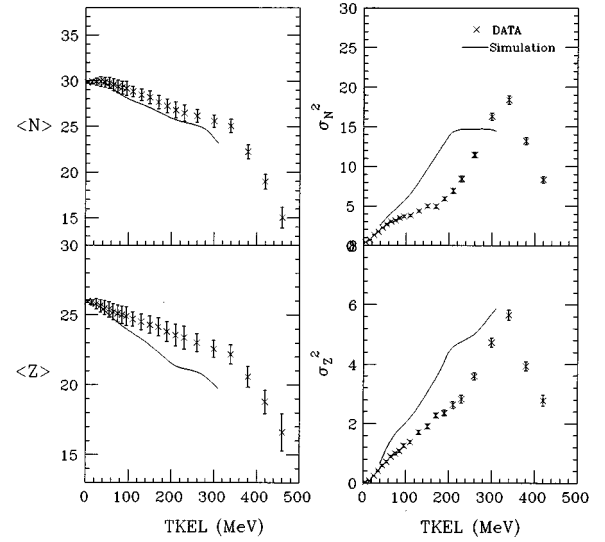


FIG. 9. The experimental values of $\langle N \rangle$, $\langle Z \rangle$, σ_Z^2 and σ_N^2 for secondary distributions, compared to the results of a Monte Carlo simulation (solid line), for the ^{56}Fe on ^{165}Ho system at 672 MeV.

mentally reconstructed primary distributions in Fig. 10. Both centroids and variances show a fairly good agreement between simulated events and real data. The differences in the secondary variances may be attributed to the random nature of the evaporation code, PACE II, which was used for evaporation corrections in two steps of the simulation.

The $E_{\text{PLF}}^*/E_{\text{tot}}^*$ centroids were determined by one-dimensional Gaussian fits and by moment analysis. Both methods yielded similar values of $E_{\text{PLF}}^*/E_{\text{tot}}^*$. The PLF excitation energy ratio determined experimentally for the 672-MeV $^{56}\text{Fe} + ^{165}\text{Ho}$ system is compared to the results of the Monte Carlo simulation in Fig. 11, for three selective bins of TKEL. The two input assumptions of the division of excitation energy are shown by the short dashed line for the as-

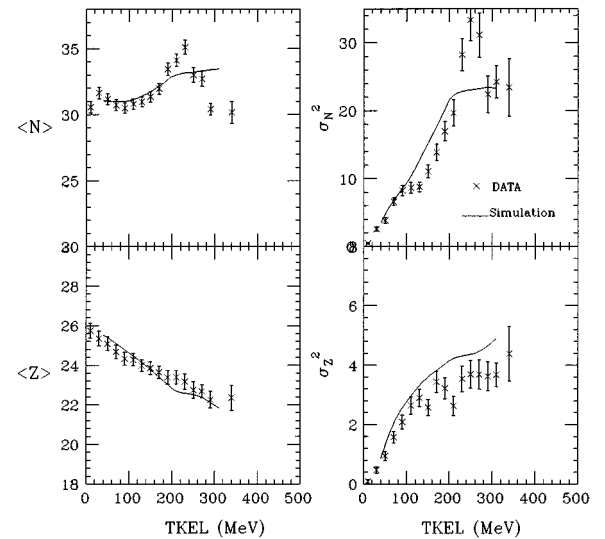


FIG. 10. The experimental values of $\langle N \rangle$, $\langle Z \rangle$, σ_Z^2 and σ_N^2 for the primary distributions obtained with kinematical reconstruction, compared to the results of a Monte Carlo simulation (solid line), for the 672-MeV ^{56}Fe on ^{165}Ho system.

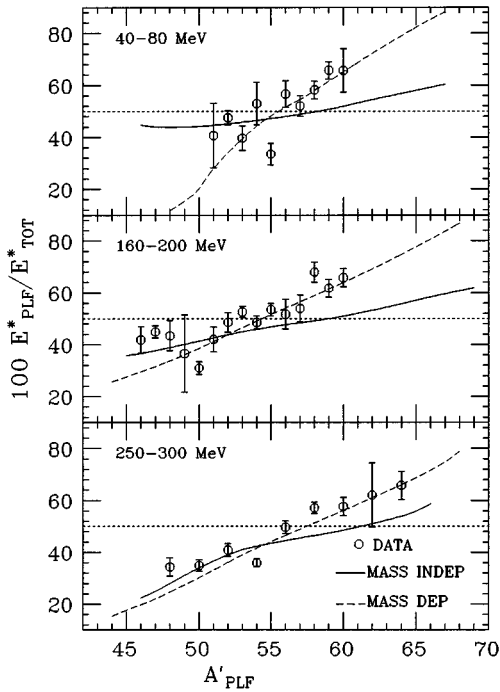


FIG. 11. The observed correlation between the PLF excitation energy ratio and the primary fragment mass (circles), compared to the results of a Monte Carlo simulation, for the reaction ^{56}Fe on ^{165}Ho at 672 MeV. The solid line indicates simulation results based on a mass-independent partition of the excitation energy (dotted line). The dashed line is the result of the simulation with a mass-dependent division of the excitation energy (average behavior of the data). The dotted line indicates the limit of excitation energy equipartition.

sumption of mass-invariant division, and by the experimental data points for the assumption of mass-dependent division. The results obtained after applying the kinematic reconstruction in the case of mass-invariant division are shown by the solid line. The results from the case of mass-dependent division are shown by the long dashed line. In the case where a mass-independent division was assumed, the deviation from the initial $E_{\text{PLF}}^*/E_{\text{tot}}^*$ value increases with increasing TKEL. This behavior is not observed for the case of mass-dependent division, where only a slight shift from the initial values of $E_{\text{PLF}}^*/E_{\text{tot}}^*$ is observed. The $E_{\text{PLF}}^*/E_{\text{tot}}^*$ ratios obtained with this latter case reproduce the experimental data better than do the $E_{\text{PLF}}^*/E_{\text{tot}}^*$ ratios obtained with the mass-independent assumption. This indicates that the correlation observed between the excitation energy sharing and the exit channel is not entirely due to instrumental effects. This is qualitatively consistent with the re-analysis of the 629-MeV $^{74}\text{Ge} + ^{165}\text{Ho}$ system by Töke *et al.* [14], where it was confirmed that some of the correlation between excitation energy division and primary fragment mass was indeed physical. However, there are still disagreements about the magnitude of this correlation.

The effects of instrumental uncertainties on the $E_{\text{PLF}}^*/E_{\text{tot}}^*$ ratios were further investigated by performing the Monte Carlo simulations of the 672-MeV ^{56}Fe on ^{165}Ho reaction with different values for the input parameters. The mass independent excitation energy division assumption was

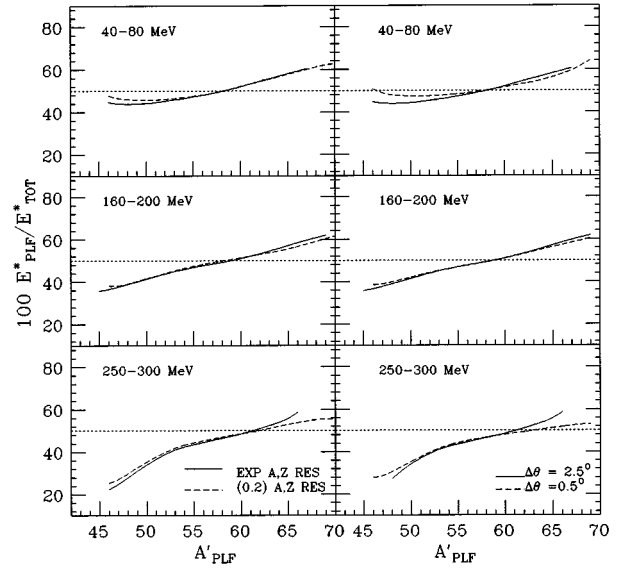


FIG. 12. The PLF excitation energy ratio predicted by a Monte Carlo simulation as a function of primary PLF mass, for the reaction ^{56}Fe on ^{165}Ho at 672 MeV. The solid lines were obtained with the charge, mass and TLF angular resolution set to the experimental values, and the dashed lines were based on a more ideal values for the Z , A , and angular resolution. The dotted line indicates the limit of excitation energy equipartition.

used since a more drastic shift was exhibited by the $E_{\text{PLF}}^*/E_{\text{tot}}^*$ when the simulation was ran with this assumption. The finite TLF angle resolution was thought to contribute significantly to the mass correlation effects on the excitation energy division. To test this hypothesis, the Monte Carlo simulation was performed with the angular resolutions $\Delta\theta_{\text{PLF}}$ and $\Delta\phi_{\text{PLF}}$ set to 0.5° , while the remaining input parameters were left unchanged. Two other parameters that are likely to introduce uncertainties in the determination of $E_{\text{PLF}}^*/E_{\text{tot}}^*$ are the charge (Z) and mass (A) resolutions of the detected PLF's. Therefore, the simulation procedure was also run with both A and Z resolutions set to 0.2 units of mass and charge, keeping the remaining parameters at their experimental values.

The $E_{\text{PLF}}^*/E_{\text{tot}}^*$ ratios obtained with the new TLF angle resolution are compared to the values obtained with the experimental TLF angle resolution in Fig. 12 (right panel) where $E_{\text{PLF}}^*/E_{\text{tot}}^*$ is plotted versus A''_{PLF} for three different ranges of TKEL. One noticeable change is observed for the low TKEL bin (40–80 MeV), where the $E_{\text{PLF}}^*/E_{\text{tot}}^*$ ratio obtained with the 0.5° resolution (dashed line) is closer to the initial assumption than the result with the 2.5° resolution (dotted line), especially for $A''_{\text{PLF}} < 58$. A small shift is also observed at high TKEL (250–300 MeV bin), where the $E_{\text{PLF}}^*/E_{\text{tot}}^*$ ratio in the 0.5° case is closer to 50% for high A''_{PLF} (> 58). No variation of $E_{\text{PLF}}^*/E_{\text{tot}}^*$ is observed for the intermediate values of TKEL (160–200 MeV bin). The same type of plot for the case of different Z and A resolutions is also shown in Fig. 12 (left panel). No sizable variation is observed at all values of TKEL. Thus, it appears that A and Z resolutions have no effect on the determination of $E_{\text{PLF}}^*/E_{\text{tot}}^*$ while TLF angle resolution introduces a slight correlation between $E_{\text{PLF}}^*/E_{\text{tot}}^*$ and A''_{PLF} . However, a prob-

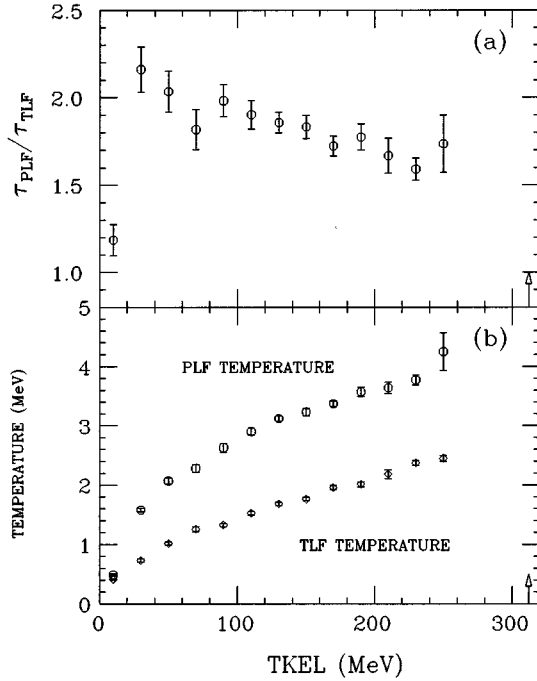


FIG. 13. The fragments nuclear temperature and the ratio of the PLF to the TLF temperatures as a function of energy loss, for the reaction ^{56}Fe on ^{165}Ho at 672 MeV. The arrow indicates the limit determined by the spherical entrance channel Coulomb barrier.

lem still remains, since the mass independent excitation energy division configuration that was used in the simulation program could not be reproduced after kinematic reconstruction.

A reanalysis of the 629-MeV $^{74}\text{Ge} + ^{165}\text{Ho}$ data was performed by Planeta *et al.* [15] with a method that does not require an exact knowledge of the experimental resolutions. In this new analysis, the correlation between excitation energy division and mass transfer were studied by plotting the average evaporated mass $\langle A'_{PLF} - A''_{PLF} \rangle$ versus the measured post-evaporation mass for different bins of energy loss. The presence of a correlation between excitation energy division and primary PLF mass was confirmed. However, this study also showed that finite resolutions were responsible for the quasiparabolic dependence of the average evaporated mass on the measured postevaporation mass of the PLF. This dependence is very weak in the current work as can be seen in Fig. 8.

VI. NUCLEAR TEMPERATURE

One of the questions addressed in the study of deep-inelastic heavy-ion reactions is whether the reaction fragments reach thermal equilibrium before they separate into a PLF and a TLF. The nuclear temperature of each fragment, as obtained from Eq. (9), is plotted as a function of energy loss in Fig. 13(b). Both temperatures increase with increasing TKEL and a steeper slope is observed below 100 MeV of TKEL. The temperature of the PLF exceeds that of the TLF at all values of the energy loss, indicating that thermal equilibrium has not been established between the two fragments. This can also be seen in Fig. 13(a), where the ratio, τ_{PLF}/τ_{TLF} , of the PLF temperature to the TLF temperature

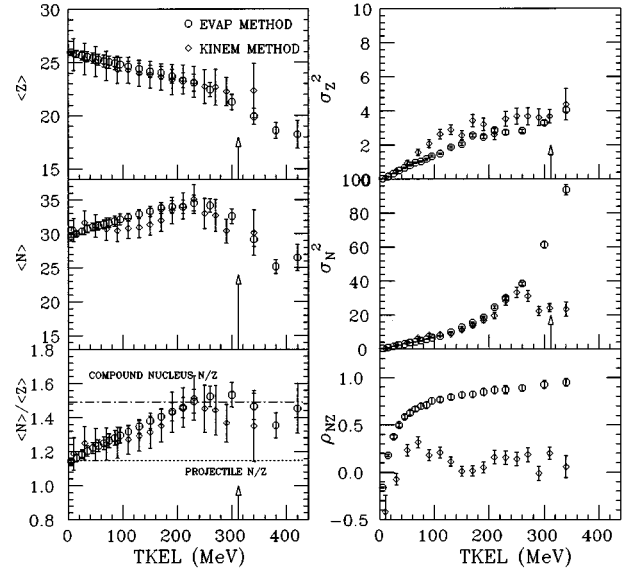


FIG. 14. The $\langle N \rangle$, $\langle Z \rangle$, $\langle N \rangle / \langle Z \rangle$, σ_Z^2 , σ_N^2 , and ρ_{NZ} values for experimental primary distributions, for the reaction ^{56}Fe on ^{165}Ho at 672 MeV. The diamonds indicate results obtained with the kinematical reconstruction method. The circles indicate the results of applying neutron evaporation corrections to the secondary distributions. The N/Z ratio of the projectile (dotted line) and the composite system (dot-dashed line) are indicated. The arrow shows the limit of energy loss determined by the spherical entrance channel Coulomb barrier.

is displayed as a function of TKEL. Figure 13(b) shows that the system evolves towards a lesser temperature gradient between the two fragments. However, it is still far from reaching equilibrium.

The study of the 505-MeV $^{56}\text{Fe} + ^{165}\text{Ho}$ reaction by Benton *et al.* [8] showed the same qualitative behavior for the temperature ratio. However, the lower bombarding energy system was closer to the limit of equal temperature than is the present system. This could imply that the interaction time of the higher bombarding energy system, which is characterized by a higher relative velocity, is not sufficiently long to allow thermalization.

VII. KINEMATIC RECONSTRUCTION VERSUS NEUTRON EVAPORATION CORRECTION

This section presents a correlation between the results of the two types of analysis conducted on the data of the 672-MeV ^{56}Fe on ^{165}Ho system. The primary mass and charge distributions that were obtained by using the kinematic coincidence technique, described in the present work, are compared to the primary distributions obtained by applying neutron evaporation corrections to the measured secondary distributions. The results of this latter analysis were reported in a previous publication [16]. The function describing the average behavior of the experimental E_{PLF}^*/E_{tot}^* ratio in terms of primary PLF mass was used to determine the PLF excitation energy when performing the neutron evaporation corrections.

The results, displayed in Fig. 14, are represented by diamonds for the kinematic reconstruction method, and by

circles for the evaporation correction method. The $\langle N \rangle$ and $\langle Z \rangle$ centroids and the $\langle N \rangle / \langle Z \rangle$ ratio obtained with the two different procedures are in agreement. The agreement in the $\langle Z \rangle$ values is consistent with the assumption that charge evaporation from the PLF is negligible for the 672-MeV $^{56}\text{Fe} + ^{165}\text{Ho}$ system. Such a result can be expected since the N/Z ratio of the PLF's produced in this reaction vary between 1.15 and 1.38 and charge evaporation becomes less important with increasing N/Z ratio.

The variances σ_Z^2 from the two techniques are in a fairly good agreement at all values of TKEL. A difference is observed for the σ_N^2 variances; those obtained with the evaporation correction method are higher for TKEL values close to the limit of the spherical entrance channel Coulomb barrier (312 MeV). This result is not surprising, since in the evaporation correction method only neutron evaporation was taken into account. In addition, in this method the mass evaporated from the PLF was evaluated by determining the average functional dependence of ΔA on an assumed E_{PLF}^* as described in Refs. [16] and [17], and the proton evaporation that may occur in regions of low N/Z ratios is unaccounted for. In the kinematic reconstruction method ΔA is evaluated exactly from experimental measurements, and ΔZ and the PLF excitation were determined by the iterative procedure described in Sec. II. This latter method is more sensitive to the details of the distribution, such as long tails, and thus gives larger variances. The correlation factor ρ_{NZ} obtained with the evaporation correction method suggests a tendency towards a correlation between proton and neutron exchange. However, the kinematics reconstruction method results in ρ_{NZ} values close to zero; this would mean that there is almost no dependence between proton and neutron exchange. It is worthwhile to point out that the nucleon exchange models of Randrup and Tassan-Got predict a gradual increase of ρ_{NZ} with increasing energy loss.

VIII. CONCLUSION

The binary character of deep-inelastic collisions was used for a kinematic reconstruction of the primary reaction, and the determination of the primary mass of the PLF was then used with the statistical evaporation code for excitation energy determination. The fraction of excitation energy stored

in the projectilelike fragment was found to exceed 50% at low energy loss, and to decrease with increasing energy loss, but without ever reaching thermal equilibrium. The same qualitative behavior of $E_{\text{PLF}}^* / E_{\text{tot}}^*$ with energy loss was observed for other systems studied with the kinematic coincidence method [8,10]. However, much larger $E_{\text{PLF}}^* / E_{\text{tot}}^*$ values were obtained for the 672-MeV ^{56}Fe on ^{165}Ho system. This is reflected in the high nuclear temperatures (up to 4 MeV) that were attained by the projectilelike fragments. The large PLF excitation energy ratios obtained for the 672-MeV ^{56}Fe on ^{165}Ho system are attributed to the higher bombarding energy. A small correlation between the PLF excitation energy ratio, $E_{\text{PLF}}^* / E_{\text{tot}}^*$ and the reaction exit channel was observed. A larger portion of excitation energy is stored in the acceptor nucleus than in the donor nucleus, however, a stronger dependence of the excitation energy division on the the direction of transfer was observed for the 505-MeV ^{56}Fe on ^{165}Ho and the 629-MeV ^{74}Ge on ^{165}Ho systems [8,10] than for the 672-MeV ^{56}Fe on ^{165}Ho system.

Monte Carlo simulations of the present experiment were performed to test the dependence of the analysis results on instrumental effects. They confirmed the existence of some correlation between the finite resolutions of the measured parameters and the calculated physical quantities. However, a further examination of the instrumental effects, by running the Monte Carlo simulation with different values for the resolution of the experimental setup, showed only a weak dependence of the simulation on the experimental parameters.

The results of the two types of analyses, evaporation correction and kinematic reconstruction, performed on the data of the 672-MeV ^{56}Fe on ^{165}Ho system are qualitatively consistent with the conclusion that the stochastic exchange of nucleons is the major contributor to energy dissipation in deep-inelastic reactions. Studies of heavy-ion reactions at intermediate energies suggest that deep-inelastic processes may still persist in this energy regime [19,20], and that a binary character of the reaction still dominates [21]. Therefore, the study of the excitation energy division between the fragments of heavy-ion reactions at intermediate bombarding energies could be a useful tool to explore the possibility of forming hot nuclear matter, and how much excitation energy a nucleus can accommodate before it breaks apart.

-
- [1] R. Babinet, B. Cauvin, J. Girard, H. Nifenecker, B. Gatty, D. Guerreau, M. Lefort, and X. Tarrago, Nucl. Phys. **A296**, 160 (1978).
- [2] B. Cauvin, R. C. Jared, P. Russo, R. P. Schmitt, R. Babinet, and L. G. Moretto, Nucl. Phys. **A301**, 511 (1978).
- [3] Y. Eyal, A. Gavron, I. Tsenurja, A. Fraenkel, Y. Eisen, S. Wald, R. Bass, C. R. Gould, G. Keyling, R. Renfordt, K. Stelzer, R. Zitmann, A. Gobbi, U. Lynen, H. Stelzer, I. Rode, and R. Bah, Phys. Rev. Lett. **41**, 625 (1978).
- [4] R. Planeta, K. Kwiatkowski, S. W. Zhou, V. E. Viola, H. Breuer, M. A. McMahan, W. Kehoe, and A. C. Mignerey, Phys. Rev. C **41**, 942 (1990).
- [5] D. Hilscher, J. R. Birkelumd, A. D. Hoover, W. U. Schröder, W. W. Wilker, J. R. Huizenga, A. C. Mignerey, K. L. Wolf, H. F. Breuer, and V. E. Viola, Jr., Phys. Rev. C **20**, 576 (1979).
- [6] Tamain, R. Chechik, H. Fuchs, F. Hanappe, M. Morjean, C. Ngô, J. Peter, M. Dakowski, B. Lucas, C. Mazur, M. Ribrag, and C. Signarbieux, Nucl. Phys. **A330**, 253 (1979).
- [7] R. Vandebosch, A. Lazzarini, D. Leach, D. K. Lock, A. Ray, and A. Seamster, Phys. Rev. Lett. **52**, 1964 (1984).
- [8] D. R. Benton, H. Breuer, F. Khazaie, K. Kwiatkowski, V. E. Viola, S. Bradley, A. C. Mignerey, and A. P. Weston-Dawkes, Phys. Lett. B **185**, 326 (1987); Phys. Rev. C **38**, 1207 (1988).
- [9] H. Sohlbach, H. Freiesleben, P. Braun-Munzinger, W. F. W. Schneider, D. Schüll, B. Kohnmeyer, M. Marinescu, and F. Phülhofer, Phys. Lett. **153B**, 385 (1985).

- [10] K. Kwiatkowski, R. Planeta, S. H. Zhou, V. E. Viola, H. Breuer, M. A. McMahan, and A. C. Mignerey, *Phys. Rev. C* **41**, 958 (1990).
- [11] V. Penumetcha, G. A. Petitt, T. C. Awes, J. R. Beene, R. L. Ferguson, F. E. Obenshain, F. Plasil, G. R. Young, and S. P. Sorensen, *Phys. Rev. C* **42** 1489 (1990).
- [12] T. C. Awes, R. L. Ferguson, R. Novotny, F. E. Obenshain, F. Plasil, S. Pontoppidan, V. Rauch, G. R. Young, and H. Sann, *Phys. Rev. Lett.* **52**, 251 (1984).
- [13] J. Randrup, *Ann. Phys. (N.Y.)* **112**, 356 (1978); *Nucl. Phys.* **A307**, 319 (1978); **A327**, 490 (1979); **A383**, 468 (1982).
- [14] J. Töke, W. U. Schröder, and J. R. Huizenga, *Phys. Rev. C* **40**, R1577 (1989); *Nucl. Instrum. Methods A* **288**, 406 (1990).
- [15] J. Töke, R. Planeta, W. U. Schröder, and J. R. Huizenga, *Phys. Rev. C* **44**, 390 (1991).
- [16] H. Madani, Ph.D. thesis (PP No. ER/40321-11); University of Maryland, 1993.
- [17] H. Madani, A. C. Mignerey, A. A. Marchetti, A. P. Weston-Dawkes, W. L. Kehoe, and F. Obenshain, *Phys. Rev. C* **51**, 2562 (1995).
- [18] H. Stege, H. J. Keim, H. A. Bösser, B. Kohlmeyer, F. Pühlhofer, and W. F. W. Schneider, *Nucl. Phys.* **A489**, 146 (1988).
- [19] B. Borderie, M. F. Rivet, and L. Tassan-Got, *Ann. Phys.* **15**, 287 (1990).
- [20] L. Tassan-Got and C. Stephan, Internal Report No. INPO-DRE-89-46, 1989; *Nucl. Phys.* **A524**, 121 (1991).
- [21] B. Lott, S. P. Baldwin, B. M. Szabo, B. M. Quednau, W. U. Schröder, J. Töke, L. G. Sobotka, J. Barreto, R. J. Charity, L. Gallamore, D. G. Sarantites, D. W. Stracener, and R. T. de Souza, *Phys. Rev. Lett.* **68**, 3141 (1992).